Hollamby, M. J., Karny, M., Bomans, P. H. H., Sommerdjik, N. A. J. M., Saeki, A., Seki, S., ... Nakanishi, T. (2014). Directed assembly of optoelectronically active alkyl--conjugated molecules by adding *n*-alkanes or -conjugated species. *Nature Chemistry*, *6*(8), 690-696. https://doi.org/10.1038/nchem.1977

Order from disorder: directed assembly of alkyl – π-conjugated molecules

Martin J. Hollamby,[1,2] Maciej Karny,[3] Paul H. H. Bomans,[4] Nico A. J. M. Sommerdjik,[4] Akinori Saeki,[5] Shu Seki,[5] Hiroyuki Minamikawa,[6] Isabelle Grillo,[7] Brian R. Pauw,[1] Paul Brown,[8] Julian Eastoe,[8] Helmuth Möhwald,[9] Takashi Nakanishi[1,3]

[1]National Institute for Materials Science (NIMS), 1-2-1 Sengen, Tsukuba 305-0047, Japan

[2]School of Physical and Geographical Sciences, Keele University, Keele, Staffordshire, ST55BG, UK

[3]Warsaw University of Technology, Pl. Politechniki 1, 00-661 Warsaw, Poland

[4]Soft Matter CryoTEM research unit, Eindhoven University of Technology, PO Box 513, 5600 MB Eindhoven, The Netherlands

[5]Department of Applied Chemistry, Graduate School of Engineering, Osaka University, Osaka 565-0871, Japan

[6]National Institute of Advanced Industrial Science and Technology (AIST), 1-1-1 Higashi, Tsukuba 305-8565, Japan

[7]Institut Max-von-Laue-Paul-Langevin, BP 156-X, F-38042 Grenoble, Cedex, France

[8]School of Chemistry, University of Bristol, Bristol BS8 1TS, UK

[9]Department of Interfaces, Max Planck Institute of Colloids and Interfaces, Research Campus Golm, Potsdam 14476, Germany

Abstract

Supramolecular assembly methods can yield ordered structures via programmed interactions between adjacent molecules. Although this is established in certain cases at the nanometre scale, general methods to direct assembly are still lacking. A straightforward approach is proposed here, using small molecule additives to direct the assembly of otherwise disordered materials. To demonstrate feasibility, hydrophobic alkylated fullerene-C_{60} molecules are employed. By selectively adding *n*-alkanes (increasing the *alkyl* content) or pristine C_{60} (increasing the *π-conjugated* content), these otherwise amorphous, disordered materials are directed to assemble as micelles, and hexagonally packed gel-fibres comprising insulated C_{60} nanowires and lamellar mesophases. The assembled structures, which occur throughout the mixtures, contain a high proportion of optoelectronically active material (domains, instead?) and can exhibit a comparably high photoconductivity. This new approach is shown to be applicable to other alkyl – π-conjugated molecules, and represents a pathway to tuneable and reproducible bulk production of self-organized soft functional materials.

Introduction

Supramolecular chemistry methods based on advanced molecular design can be used to generate complex structures, over a range of length-scales, programmed by the chemical structure of the component molecules. Examples include DNA origami,[1,2] supramolecular polymers,[3,4] or supra-amphiphiles[5] often exhibiting intriguing stimuli-responsive properties. However, general routes for the directed assembly in a controllable manner of otherwise disordered materials have yet to be identified.[6,7] Overcoming this hurdle is of particular importance for development of molecular optoelectronic materials, for which molecular alignment and the presence of defects or deep traps at grain boundaries directly affect device performance.[8] A common concern is that molecules with otherwise excellent intrinsic properties frequently form suboptimal assembly structures in their native state, limiting applications.[6] One solution may be provided by supramolecular liquid crystalline materials,[9–11] although enhanced functionality provided by the π-conjugated units in the component molecules, has yet to be fully demonstrated. One limiting factor may be the relatively low π-conjugated content in many of these systems.[12]

Here, we (I would say “Here is introduced”) introduce an alternative straightforward approach to direct the assembly of π-conjugated molecules from an amorphous state into useable ordered materials. Alkyl chains (*e.g.* long, branched) are routinely attached to optoelectronically active π-conjugated molecules to facilitate solution processing and to tune self-assembly.[11–15] When the alkyl chains are attached to just one side of the π-conjugated moiety, the result is an asymmetric “hydrophobic amphiphile” with two immiscible groups.[16–19] By introducing additives with a selective affinity towards either moiety, it was expected that a multitude of complex ordered fluids, for example micelles, gels and two-component liquid crystals, might be accessible, analogous to those encountered in classical hydrophobic-hydrophilic amphiphile assemblies.[20]

To demonstrate the feasibility of this approach, we (I would write “apersonally”) initially focus on two hydrophobic alkylated fullerene-C_{60} derivatives. The discrepancy in non-covalent interaction strength between the π-conjugated fullerene and the attached alkyl

chains has been previously used to control molecular self-organisation in additive-free states.[18,19] However, here we chose alkylated C_{60} derivatives (*vide infra*) that are inherently disordered, to emphasise the power of the new approach. By the addition of *n*-alkanes or pristine C_{60}, which either increase the total alkyl or π-conjugated content of the system, the alkylated C_{60} derivatives are directed to assemble into different ordered structures. The driving force for nanoscale phase separation is the immiscibility of C_{60} with alkanes (or alkyl chains).[15,21] This powerful principle, which is shown to be applicable to other alkyl – π-conjugated molecules, provides a tuneable route to direct disordered yet functional π-conjugated molecules to assemble into useful materials.

Results

Micelles

The alkylated C_{60} derivative **1** (Fig. 1a) was synthesized and purified using previously described methods.[19,22] **1** is a liquid at room temperature and is fully miscible with *n*-hexane, forming dark solutions (*e.g.* photo, Fig. 1a) of relatively low viscosity. This miscibility is counterintuitive given the low solubility of pristine C_{60} in *n*-alkanes (< 0.1 mM).[21] Solubility enhancements are often observed in molecules comprising two parts with widely differing solvophobicity[23] including surfactants[24], semifluorinated alkanes[16] or block copolymers.[17] Molecules like this self-assemble in solution, so as to limit contacts between the solvophobic part and solvent. It was hypothesised that the increase in solubility observed for hydrophobic amphiphile **1** might also be due to clustering to minimize unfavourable interactions between C_{60} groups and *n*-alkane molecules.

UV-vis absorption spectra of **1** in *n*-hexane (Fig. 1b), *n*-octane, *n*-decane and toluene (Supplementary Fig. S1a-c) in the region 630-765 nm revealed several maxima, typical for C_{60} derivatives prepared by this route.[22] Increasing concentration from 1 to 11 wt% of **1** led to broadening and bathochromic shifts for all peaks in every solvent studied, consistent with aggregation. The magnitude of the shift with increasing concentration was strongly solvent dependent, with the largest shifts noted for *n*-hexane, followed by *n*-octane, *n*-decane and

toluene (instead you could write “following the order *n*-hexane > *n*-octane > *n*-decane > toluene”). This points to a trend in aggregation mirroring the difference in cohesive energy between the C_{60} parts of **1** and solvent.[21]

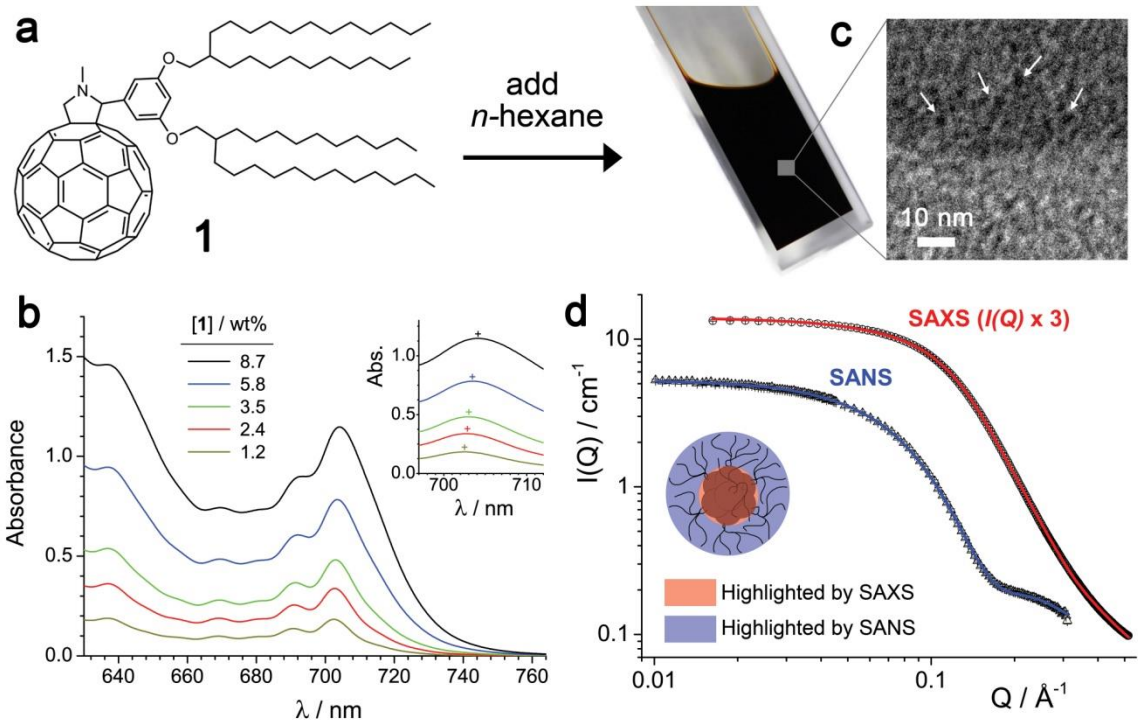

Figure 1

Cryogenic transmission electron microscopy (*cryo*-TEM) confirmed the existence of clusters in *n*-decane (Fig. 1c and Supplementary figure S2). Owing to higher electron density of C_{60}, the dark spherical regions (indicated with arrows, Fig. 1c) are likely to be C_{60}-rich cores of core-shell micelles. The micelle cores appear spherical and polydisperse in size, with an average diameter of 2.5 ± 0.3 nm (see Supplementary Fig. S2), which is indicative of small aggregates containing around 6 molecules of **1**.

To further investigate the solutions and to evaluate the influence of concentration and solvent type on micellar properties, small-angle X-ray (SAXS) and neutron (SANS) scattering were applied (Fig. 1d and Supplementary Fig. S3). X-rays scatter from nanoscale electron density inhomogeneities within samples, here effectively highlighting the clustered C_{60} parts of **1** in the lower electron density *n*-alkane matrix. Conversely, neutrons scatter owing to

interactions with sample nuclei, and in particular scatter very differently from hydrogen and deuterium nuclei.[25] SANS from **1** added to perdeuterated D-solvents thereby highlights domains comprising H-alkyl chains.

The SAXS and SANS data for **1** in *n*-hexane are shown in Fig. 1d. Both datasets exhibit a region at low *Q* where *I(Q)*, scales as Q^0, followed by a decay. The decay onsets are inversely related to the radius of gyration of the scattering objects.[25,26] As the first decay in the SANS signal occurs at lower *Q* values than in SAXS, the domains scattering neutrons are effectively larger than those probed by the X-ray experiment. The data are therefore consistent with a core-shell micellar structure as suggested by *cryo*-TEM, with C_{60}-rich cores and alkyl-rich shells (*e.g.* inset schematic, Fig. 1d). The onset of the decay in the SAXS data corresponds C_{60} micellar core radii, whereas the first decay in the SANS data represents an overall core+shell dimension. In the SANS data the second decay at around $Q \approx 0.22$ Å^{-1} is related to the shell thickness.

SAXS was used to investigate the effect of solvent type (*n*-hexane, *n*-decane, toluene) and concentration (2 - 22 wt%) on micelle size. The scattering objects were modelled as a polydisperse distribution of spherical core-shell micelles (see Supplementary Information). Fitted data and size distributions are shown in Supplementary Figure S3 and fit parameters for SAXS and SANS data are given in Supplementary Tables S1 and S2 respectively. Micelle radii, R_{vw} increased with concentration and were larger in *n*-hexane than in *n*-decane, in line with the changes observed in UV-vis spectra. Average sizes in *n*-hexane and *n*-decane (R_{vw} = 12.7 Å and 9.4 Å respectively – do not mix up units - Martin change all the dimensions reported to be in the same units in the whole paper – use nm not A – you can keep Q in A-1 however) are in agreement with the results from cryo-TEM (core diameter ~ 3 nm). In toluene comparatively little aggregation was detected, consistent with the known higher solubility of C_{60} in this solvent.

In summary, the multi-technique combination of UV-vis, *cryo*-TEM and SAXS/SANS clearly demonstrate that solvophobicity for *n*-alkanes of the π-conjugated parts of **1** is sufficient to drive assembly into structured micelles.

Gel fibres

The study was broadened to **2** (Fig. 2a), which is a disordered amorphous solid at room temperature.[19] Gentle heating greatly increased the miscibility of **2** with *n*-hexane (Fig. 2b). SAXS data from a sample of 19.8 wt% **2** in *n*-hexane at 55 °C shown in Fig. 2c are similar to observations with mixtures of **1** (*e.g.* Fig. 1d), indicating the presence of micelles (*e.g.* schematic illustration, Fig. 2c). These micelles have R_{vw} = 11 Å but a higher polydispersity than micelles of **1**, which may indicate more elongated structures.

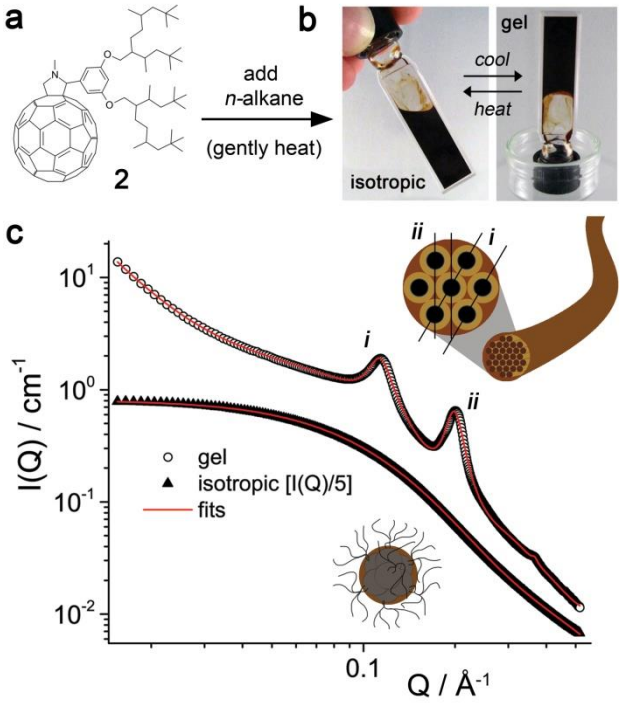

Figure 2

Interestingly, the samples gelled upon cooling from the isotropic state (Fig. 2b). This process was reversible, with a transition point, T_{trans} just above room temperature (Supplementary Fig. S4). SAXS data taken at 5 °C (<<T_{trans}) are shown in the upper plot in Fig. 2c. In comparison with the data at 55 °C, an increased *I(Q)* at low *Q* and the development of several peaks are noted, indicating an increased order over length scales probed by SAXS (15 – 600 Å) . The peaks marked as ***i*** and ***ii*** correspond to *d*-spacings of 55

and 31 ± 1 Å respectively. The difference between *d*-spacings is approximately √3, suggesting a hexagonally-ordered columnar lattice of **2** in which the C_{60} portions are in the column centres (*e.g.* inset schematic illustration, Fig. 2c).[27]

To further characterise the gel structure in *n*-hexane, polarized optical microscopy (POM) and temperature-controlled X-ray diffraction (XRD) were applied (Fig. 3a). Firstly observations were made in the absence of polarizers: at [**2**] = 19.8 wt%, a network of bundled fibres was observed. Next the polariziers were introduced in the standard PM configuration: the fibres exhibited textures indicating internal order (for isotropic state, see Supplementary Fig. S5). Temperature-controlled XRD (Fig. 3a: T = 0 °C, [**2**] = 28.7 wt%) also showed peaks ***i*** and ***ii***, at *d*-spacings of 49.9 and 29.0 ± 2 Å. Additionally, multiple smaller peaks and shoulders were also noted (***iii***, ***iv*** and ***v*** on Fig. 3a positions, with corresponding *d*-spacings are given in Supplementary Table S3). The slight difference in the position of peaks ***i*** and ***ii*** determined by SAXS and XRD may be due to the limit of detection ($2\theta \approx 1.6$) of the XRD setup or the difference in concentration (*vide infra*).

The ratio in positions of the peaks ***i***-***v*** determined by XRD is approximately 1:√3: √4: √7: √12, as expected for the 2D *p6mm* hexagonal symmetry group.[27] This indicates that **2** assembles into hexagonally ordered columnar domains in the gel. Whereas, hexagonal ordering is commonly noted in thermotropic C_{60}-containing liquid crystals[12], it is uncommon for lyotropic C_{60}-containing gels[28,29] and is particularly notable given the lack of gel-promoting hydrogen bonding moieties or tertiary gelators. The two sharp peaks in the region $2\theta \approx 9°$ are likely to correspond to C_{60}-C_{60} spacing of around 10 Å, indicating a relatively high level of ordering of the C_{60} moieties. Neighbouring fullerenes can therefore approach to within 3 Å, enabling effective charge transport along the columns. From the SAXS and XRD data, the inter-columnar spacing is 60 ± 4 Å. As this is larger than twice the length of **2** (≈ 25 Å), the hexagonally-packed columns of C_{60} are likely to be separated by alkyl regions which also contain interpenetrated *n*-hexane molecules (*cf.* C_{60} wires surrounded by insulator).

The SAXS data in Fig. 2c were therefore modelled as a network of fibres composed of hexagonally spaced monodisperse cylinders representing the C_{60} columns (see

Supplementary Information). Related models have been used to describe gels of conducting polymers.[30] The network fractal dimension (2.7) is consistent with the overlapped fibre bundles observed by POM. The cylinder radius (16 Å) was similar to the micelle radii for **1** and **2**, suggesting fibre growth from the clustered micellar state.

The ability of **2** to gel other solvents was studied. Gels did not form with toluene, chloroform or cyclohexane, but did with other *n*-alkanes (*n*-octane, *n*-decane). Using near-infrared turbidity measurements (Supplementary Fig. S4), the gel formation temperature T_{trans} was found to be decrease with increasing *n*-alkane chain length and to increase with the concentration of **2**. XRD data (Supplementary Fig. S7a,b and Table S3) point to similar gel structures with all *n*-alkanes used, within the concentration range of 16.5 to 42 wt%. This assertion was backed up by *cryo*-TEM images taken at the onset of gel formation in *n*-decane (Supplementary Figure S6). Both micelles and more ordered structures with two primary spacings (d_1 and d_2) of approximately 4.8 and 3.0 nm are clear in the images. However, one subtle change noted using XRD was the positional shift to higher 2θ value and slight broadening of peak ***i*** with increasing alkane chain length (2θ = 1.92 and 1.77 for ~20 wt% **2** in *n*-decane and *n*-hexane) and at higher concentrations (2θ = 1.96 for 42 wt% **2** in *n*-decane). This may indicate a uniaxial contraction arising from the reduced affinity of *n*-decane versus *n*-hexane towards the branched alkyl chains of **2** (Supplementary Fig. S7c,d).

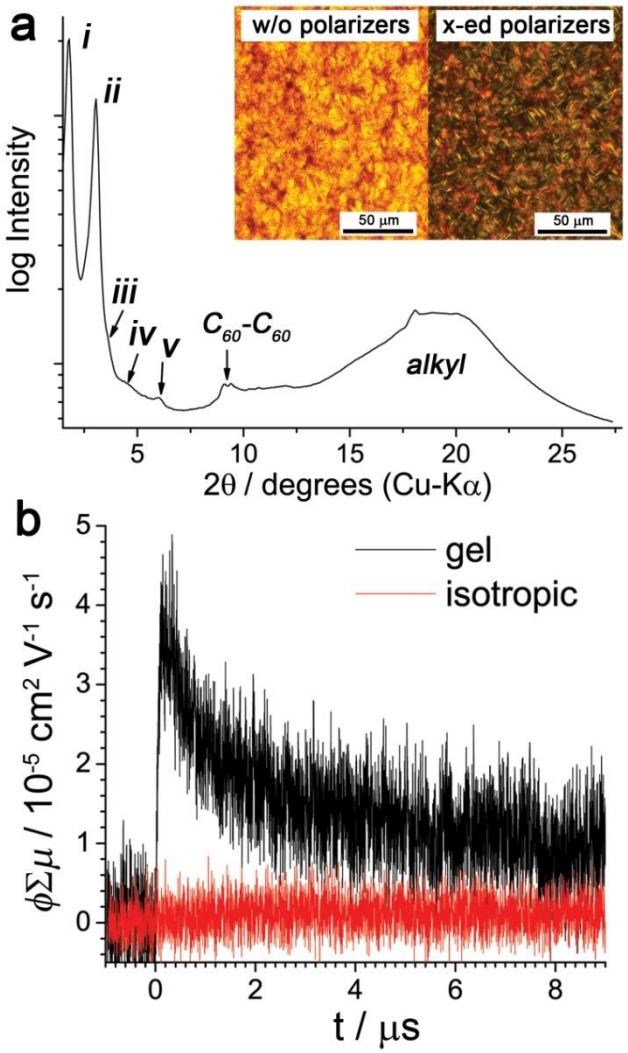

Figure 3

Flash-photolysis time resolved microwave conductivity (FP-TRMC)[31] was used to probe the photoconductivity of the C_{60}-rich columnar domains. Measurements of the transient photoconductivity $\phi\Sigma\mu$ for a sample of **2** with *n*-decane are shown in Fig. 3b (ϕ represents the quantum efficiency of the charge carrier generation and $\Sigma\mu$ represents the sum of the nanometre-scale charge carrier mobilities).[31] FP-TRMC measurements in the solvated state are difficult and typically suffer from low signal and a higher background noise due to the insulating solvent content. Despite this, a clear signals were detected for the gels that were not present for the isotropic clusters (Fig. 3b). The photoconductivity maximum ($\phi\Sigma\mu_{max}$ = 3.5 x 10^{-5} cm^2 V^{-1} s^{-1}) was of similar order as that for solid crystalline C_{60} derivatives studied

using the same technique, including PCBM ([6,6]-phenyl-C_{61}-butyric acid methyl ester, 2.8 – 14 x 10^{-5} cm^2 V^{-1} s^{-1}).[32,33] While TRMC evaluates carrier mobility at the nanometer scale, the results indicate that the fibre network transports charge and might be applicable in flexible optoelectronic applications in the gelled state,[34] with the potential for unique self-healing or thermally-induced on-off switching properties.

The results above therefore confirm the existence of true solvated-state alkyl – π-conjugated hydrophobic amphiphilicity and provide the first example of the directed assembly of alkyl – π-conjugated molecules into well-defined structures in the bulk solvated state via the addition of only *n*-alkanes. Related approaches using different solvents[35–37] or the addition of anti-solvent[38,39] to self-organize functional supramolecular structures out of solution have previously been reported, but are not always well understood, can be limited by solubility, and furthermore are conceptually different to this current approach. These results indicate a type of directed assembly similar to higher order assemblies of more conventional hydrophobic-hydrophilic surfactants, significantly extending the general concept of solvophobic - solvophilic balance for inducing and tuning self-assembly in low dielectric and non-aqueous media. The different aggregation extent of **1** and **2** is expected, as the ability of the alkyl chain chemistry to tune chain-chain and chain-solvent interactions has also been noted for conventional surfactants.[40,41] It is likely that increased branching reduces the interaction strength between alkyl chains and *n*-alkanes and weakens the ability to interfere in π-π interactions between neighbouring C_{60} units, yielding larger assemblies. The coupling of in-depth molecular design with the additive-directed assembly approach appears to provide a powerful new way to construct assembled molecular materials with high functionality and complexity.

To further demonstrate the generality of our approach, fullerene-C_{70} derivative **3** and azobenzene derivative **4** (Supplementary Fig. S8) were investigated. These represent larger (C_{70}) and smaller (azobenzene) π-conjugated systems than C_{60}. Both derivatives are liquid at room temperature, but after the addition of *n*-alkanes, clusters were detected by SAXS (Supplementary Fig. S8). Micelle radii were larger for **3** (12.2 Å) than for **1** (9.4 Å) under

similar conditions (~20 wt% in *n*-decane) and were smaller for **4** (5.0 Å) respectively (Supplementary Table S4). Reducing the concentration of **3** in *n*-decane was found to also reduce micelle size (Supplementary Fig. S8), in line with the results seen for **1** in *n*-hexane. It is therefore clear that the ability to direct assembly of alkyl – π-conjugated molecules using *n*-alkanes is not only limited to C_{60}-containing species, and that the strength of interaction between the π-conjugated moieties is a key control parameter in assembly.

Lamellar mesophases

Additives with higher affinities for the C_{60} part than for alkyl chains are also expected to drive assembly; for example, the addition of pristine C_{60} to **1**. Coassembly structures of C_{60} with polymers[42,43] and planar π-conjugated groups such as porphyrins[44] have been described,[18,45] but to our knowledge the coassembly of pristine C_{60} with C_{60} derivatives to direct assembly has yet to be realized. Pure **1** is a liquid at room temperature, when C_{60} and **1** were mixed in toluene at molar ratios of C_{60}:**1** of 1:2 and 1:10, UV-vis spectroscopy indicated little interaction between the two species (Supplementary Figure S9). However, thick pastes were formed after removal of the solvent by evaporation.

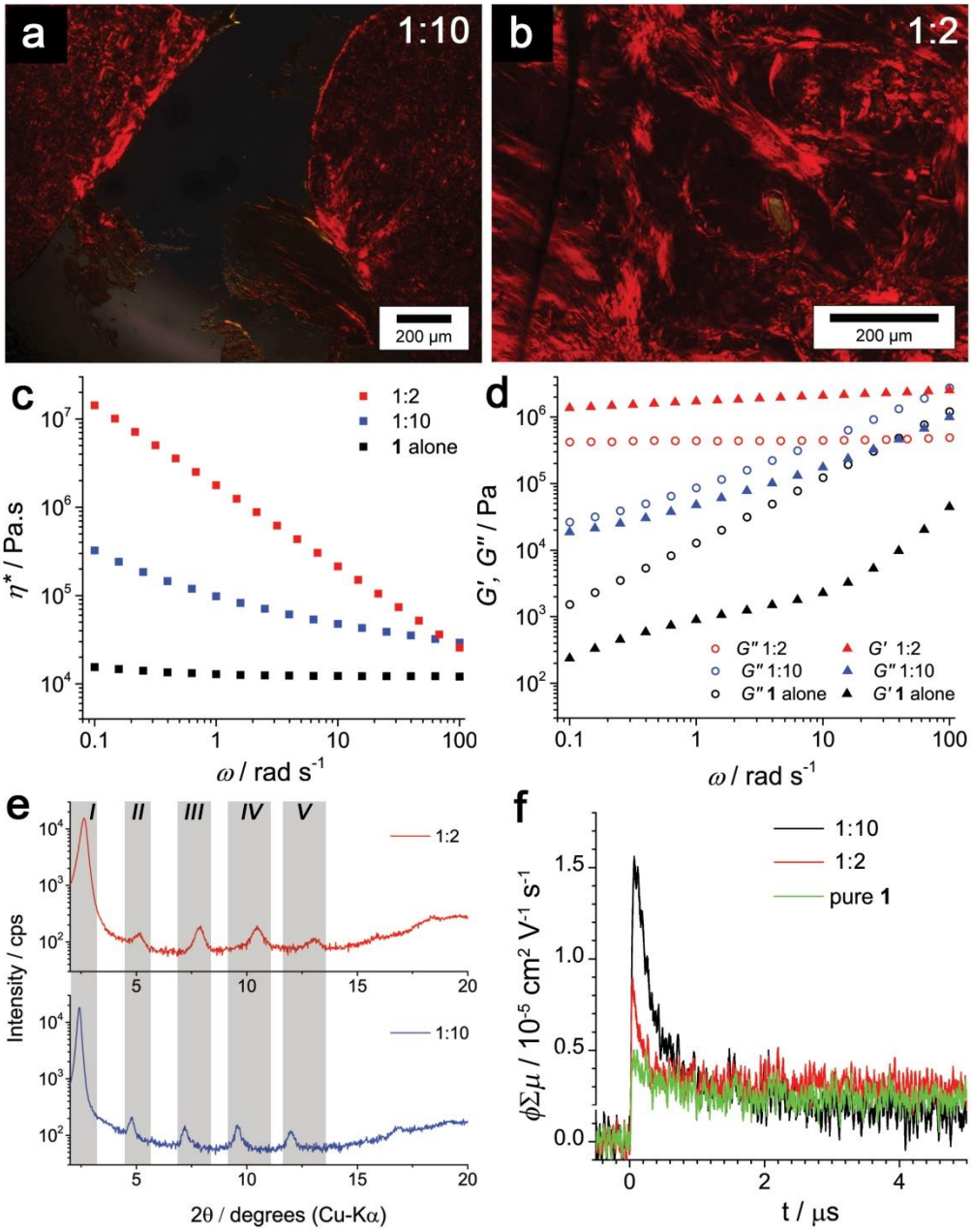

Figure 4

POM images of the pastes (Fig. 4a,b) exhibited marbled textures similar to those noted for smectic phases of fullerene-containing thermotropic liquid crystals.[12,13,15] The rheological behaviour (Fig. 4c,d) of the pastes was distinctly different to that for pure **1**, with higher complex viscosity η^*, storage modulus *G'*, and loss modulus *G"* values throughout almost the entire applied angular frequency (ω) range. The pastes shear thin as indicated by the reduction in η^* with increasing ω. Similarly to **1**, 1:10 exhibits viscoelastic behaviour, with *G"*

> *G'*. However, solid-like behaviour is noted for 1:2, with *G''* < *G'* at this strain amplitude (0.1%). In general, these results point to large increases in intermolecular interactions on adding C_{60} to **1**, in line with directed assembly formation.

XRD (Fig. 4e) and TEM (Fig. 5) confirmed the existence of extended lamellar domains. The lack of any discernible peaks in the XRD corresponding to the fcc phase of C_{60} suggests it is mostly incorporated into the lamellar structure. Several evenly-spaced peaks (labelled ***I-V*** on Fig. 4e) were detected, corresponding to the 001 - 005 reflections of a lamellar mesophase.[27] For 1:2 mixtures the peaks are broader and shifted to higher 2θ values than for the 1:10 sample, indicating of a smaller lamellar spacing (34 *vs.* 37 Å) and a reduced persistence length[46] of the lamellar structure (190 *vs.* 310 Å). As the 1:2 sample contains proportionally more C_{60}, there may also be more C_{60} incorporated within the lamellar structure, which would lead to closer contact between layers due to a reduction in the amount of the alkyl "spacer" group. FP-TRMC (Fig. 4f) measurements gave $\phi\Sigma\mu_{max}$ = 0.9 and 1.5 x 10^{-5} cm^2 V^{-1} s^{-1} for the 1:2 and 1:10 blends respectively, which are both higher than that obtained for pure **1** (0.4 x 10^{-5} cm^2 V^{-1} s^{-1}). Interestingly, the highest $\phi\Sigma\mu_{max}$ was obtained for 1:10, for which the more extensive mesophases were noted by XRD.

Echoing the results from XRD, TEM images of 1:10 show lamellar domains with a persistence length of ≥20 nm in the lamellar growth direction, and at least 50 nm in the lamellar plane (Fig. 5a). Within the layers, dark regions corresponding to stacked C_{60} units can be distinguished, which are interdigitated at an angle of ~60° (Fig. 5b). Lamellar and C_{60}-C_{60} *d*-spacings were 3.6 and 1.1 nm respectively (FFT, Fig. 5c), in agreement with the XRD results.

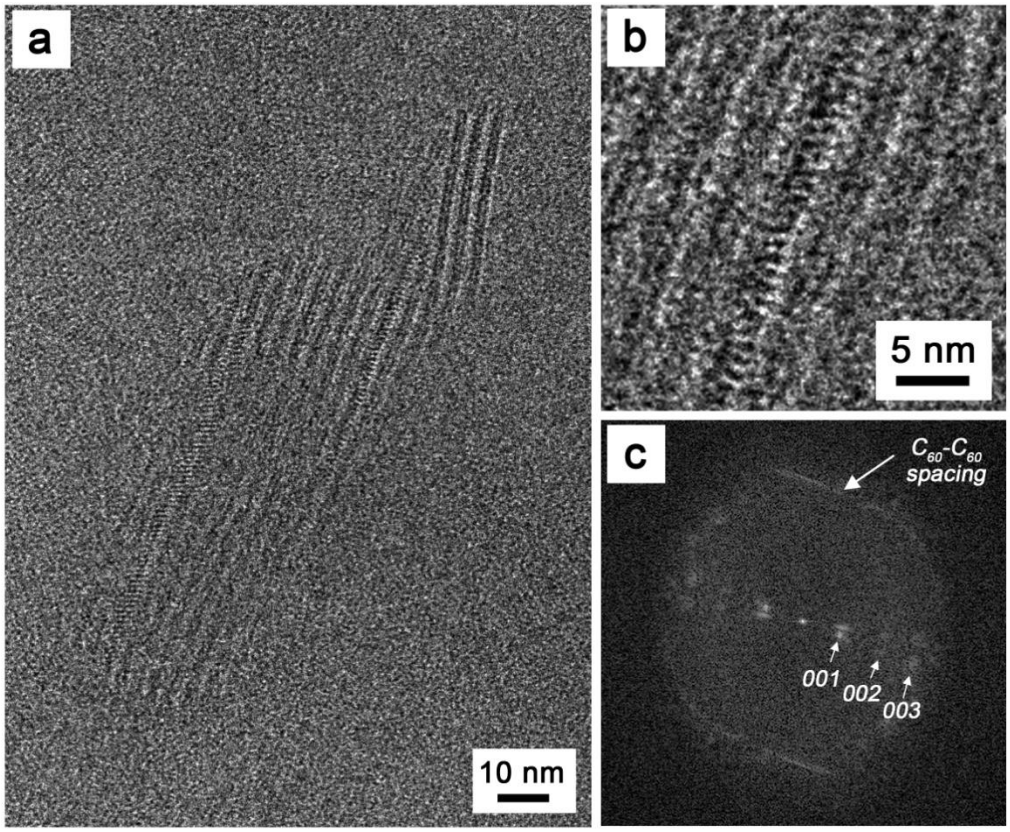

Figure 5

Clearly addition of C_{60} to alkylated C_{60} derivatives is also able to induce assembly, just as the addition of *n*-alkanes (Fig. 6). That such a small quantity of C_{60} (1:10 contains 4.4 wt% C_{60}) causes such a significant change in both the nanoscale and bulk properties the initially liquid material is very interesting, and perhaps points to the C_{60} units acting as seeds for mesophase growth. When generalised for other additives and alkyl – π-conjugated molecules, this can become an extremely useful assembly tool of particular relevance to the developing field of functional organic fluids.[47,48] With this in mind, a different C_{60} derivative **5** was synthesised, bearing a single 2-decyl-1-tetradecanol group exchanged with the methyl group on PCBM (see Supplementary Synthesis). Like **1**, molecule **5** is a liquid at room temperature: adding either C_{60} or $PC_{61}BM$ to **5** resulted in the formation of lamellar-type assemblies, as verified by XRD and POM results (Supplementary Figure S10). While this

new system has yet to be studied in depth, it is clear that the reported phenomenon is apparently general for molecules and additives form these broad classes.

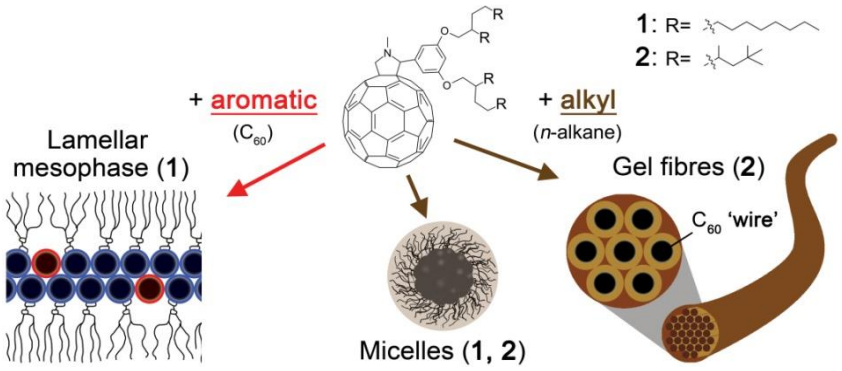

Figure 6

Discussion

The thermodynamic origin of aggregation for conventional hydrophobic-hydrophilic amphiphiles is an appropriate balance between hydrophilic and hydrophobic interactions. Here, that concept is generalised to encompass solvophilicity and solvophobicity within hydrophobic amphiphiles and antipathy induced by combinations of alkyl and π-conjugated moieities is also shown to drive self-assembly. The extent of aggregation can be tuned using a balance of alkyl and π-conjugated components, to generate materials of different micro- and macroscopic properties. This new concept therefore promises a multitude of complex fluids and phases, with the additional benefit of localised and aligned π-conjugated content, and potential for unique and switchable optoelectronic properties. It has notable advantages over existing solution-state, hydrophilic-hydrophobic C_{60}-amphiphile strategies[12,49,50] owing to ease of application, increased solution processability of the materials and uniformity for bulk-scale assemblies. Clearly the combination of molecular design strategies[1–5] possible with this approach will provide a potent and robust method to construct and optimise functional materials based on π-conjugated molecules, with nanoscale control.

References

1. Rothemund, P. W. K. Folding DNA to create nanoscale shapes and patterns. *Nature* **440,** 297–302 (2006).
2. Sobczak, J.-P. J., Martin, T. G., Gerling, T. & Dietz, H. Rapid Folding of DNA into Nanoscale Shapes at Constant Temperature. *Science* **338,** 1458–1461 (2012).
3. Aida, T., Meijer, E. W. & Stupp, S. I. Functional Supramolecular Polymers. *Science* **335,** 813–817 (2012).
4. Du, G., Moulin, E., Jouault, N., Buhler, E. & Giuseppone, N. Muscle-like Supramolecular Polymers: Integrated Motion from Thousands of Molecular Machines. *Angew. Chem. Int. Ed.* **51,** 12504–12508 (2012).
5. Wang, C., Wang, Z. & Zhang, X. Amphiphilic Building Blocks for Self-Assembly: From Amphiphiles to Supra-amphiphiles. *Acc. Chem. Res.* **45,** 608–618 (2012).
6. Henson, Z. B., Müllen, K. & Bazan, G. C. Design strategies for organic semiconductors beyond the molecular formula. *Nat. Chem.* **4,** 699–704 (2012).
7. Tang, C., Lennon, E. M., Fredrickson, G. H., Kramer, E. J. & Hawker, C. J. Evolution of Block Copolymer Lithography to Highly Ordered Square Arrays. *Science* **322,** 429–432 (2008).
8. Altoe, V., Martin, F., Katan, A., Salmeron, M. & Aloni, S. Electron Microscopy Reveals Structure and Morphology of One Molecule Thin Organic Films. *Nano Lett.* **12,** 1295–1299 (2012).
9. Pisula, W., Feng, X. & Müllen, K. Tuning the Columnar Organization of Discotic Polycyclic Aromatic Hydrocarbons. *Adv. Mater.* **22,** 3634–3649 (2010).
10. Percec, V. *et al.* Self-organization of supramolecular helical dendrimers into complex electronic materials. *Nature* **419,** 384–387 (2002).
11. Saez, I. M. & Goodby, J. W. Supermolecular liquid crystals. *J. Mater. Chem.* **15,** 26–40 (2005).
12. Guillon, D., Donnio, B. & Deschenaux, R. in *Supramolecular Chemistry of Fullerenes and Carbon Nanotubes* (Martín, N. & Nierengarten, J.-F.) 203–235 (Wiley-VCH Verlag GmbH & Co. KGaA, 2012).

13. Vergara, J. *et al.* Liquid-Crystalline Hybrid Materials Based on [60]Fullerene and Bent-Core Structures. *Angew. Chem. Int. Ed.* **50,** 12523–12528 (2011).
14. Li, H., Choi, J. & Nakanishi, T. Optoelectronic Functional Materials Based on Alkylated-π Molecules: Self-Assembled Architectures and Nonassembled Liquids. *Langmuir* **29,** 5394–5406 (2013).
15. Zhong, Y.-W., Matsuo, Y. & Nakamura, E. Lamellar Assembly of Conical Molecules Possessing a Fullerene Apex in Crystals and Liquid Crystals. *J. Am. Chem. Soc.* **129,** 3052–3053 (2007).
16. Binks, B. P., Fletcher, P. D. I., Kotsev, S. N. & Thompson, R. L. Adsorption and Aggregation of Semifluorinated Alkanes in Binary and Ternary Mixtures with Hydrocarbon and Fluorocarbon Solvents. *Langmuir* **13,** 6669–6682 (1997).
17. Blanazs, A., Armes, S. P. & Ryan, A. J. Self-Assembled Block Copolymer Aggregates: From Micelles to Vesicles and their Biological Applications. *Macromol. Rapid Comm.* **30,** 267–277 (2009).
18. Nakanishi, T. Supramolecular soft and hard materials based on self-assembly algorithms of alkyl-conjugated fullerenes. *Chem. Commun.* **46,** 3425–3436 (2010).
19. Li, H. *et al.* Alkylated-C_{60} based soft materials: regulation of self-assembly and optoelectronic properties by chain branching. *J. Mater. Chem. C* **1,** 1943–1951 (2013).
20. Israelachvili, J. in *Surfactants in Solution* (Mittal, K. L. & Bothorel, P.) 3–33 (Springer US, 1987). at <http://link.springer.com/chapter/10.1007/978-1-4613-1831-6_1>
21. Ruoff, R. S., Tse, D. S., Malhotra, R. & Lorents, D. C. Solubility of fullerene (C_{60}) in a variety of solvents. *J. Phys. Chem.* **97,** 3379–3383 (1993).
22. Kordatos, K., Da Ros, T., Prato, M., Bensasson, R. V. & Leach, S. Absorption spectra of the mono-adduct and eight bis-adduct regioisomers of pyrrolidine derivatives of C_{60}. *Chem. Phys.* **293,** 263–280 (2003).
23. Sedov, I. A., Stolov, M. A. & Solomonov, B. N. Solvophobic effects and relationships between the Gibbs energy and enthalpy for the solvation process. *J. Phys. Org. Chem.* **24,** 1088–1094 (2011).

24. Moyá, M. L., Rodríguez, A., Graciani, M. del M. & Fernández, G. Role of the solvophobic effect on micellization. *J. Colloid Interf. Sci.* **316,** 787–795 (2007).
25. Hollamby, M. J. Practical applications of small-angle neutron scattering. *Phys. Chem. Chem. Phys.* **15,** 10566–10579 (2013).
26. Guinier, A. *Ann. Phys.* **12,** 161–237 (1939).
27. Hyde, S. T. in *Handbook of applied surface and colloid chemistry* **1-2,** 299–332 (John Wiley & Sons, Inc., 2001).
28. Ishi-i, T., Ono, Y. & Shinkai, S. Chirally-Ordered Fullerene Assemblies Found in Organic Gel Systems of Cholesterol-Appended [60]Fullerenes. *Chem. Lett.* **29,** 808–809 (2000).
29. Yang, X. *et al.* Self-assembly of a new C_{60} compound with a L-glutamid-derived lipid unit: formation of organogels and hierarchically structured spherical particles. *Soft Matter* **7,** 3592–3598 (2011).
30. Newbloom, G. M., Kim, F. S., Jenekhe, S. A. & Pozzo, D. C. Mesoscale Morphology and Charge Transport in Colloidal Networks of Poly(3-hexylthiophene). *Macromolecules* **44,** 3801–3809 (2011).
31. Saeki, A., Seki, S., Takenobu, T., Iwasa, Y. & Tagawa, S. Mobility and Dynamics of Charge Carriers in Rubrene Single Crystals Studied by Flash-Photolysis Microwave Conductivity and Optical Spectroscopy. *Adv. Mater.* **20,** 920–923 (2008).
32. Babu, S. S., Saeki, A., Seki, S., Möhwald, H. & Nakanishi, T. Millimeter-sized flat crystalline sheet architectures of fullerene assemblies with anisotropic photoconductivity. *Phys. Chem. Chem. Phys.* **13,** 4830–4834 (2011).
33. Zhang, X. *et al.* Flowerlike supramolecular architectures assembled from C_{60} equipped with a pyridine substituent. *Chem. Commun.* **46,** 8752–8754 (2010).
34. Babu, S. S., Prasanthkumar, S. & Ajayaghosh, A. Self-Assembled Gelators for Organic Electronics. *Angew. Chem. Int. Ed.* **51,** 1766–1776 (2012).
35. Park, C., Song, H. J. & Choi, H. C. The critical effect of solvent geometry on the determination of fullerene (C_{60}) self-assembly into dot, wire and disk structures. *Chem. Commun.* 4803–4805 (2009). doi:10.1039/b909888g

36. Lei, T. & Pei, J. Solution-processed organic nano- and micro-materials: design strategy, growth mechanism and applications. *J. Mater. Chem.* **22,** 785–798 (2012).
37. Vera, F. *et al.* Microstructured objects produced by the supramolecular hierarchical assembly of an organic free radical gathering hydrophobic-amphiphilic characteristics. *Chem. Sci.* **3,** 1958–1962 (2012).
38. Sathish, M., Miyazawa, K., Hill, J. P. & Ariga, K. Solvent Engineering for Shape-Shifter Pure Fullerene (C_{60}). *J. Am. Chem. Soc.* **131,** 6372–6373 (2009).
39. Balakrishnan, K. *et al.* Effect of Side-Chain Substituents on Self-Assembly of Perylene Diimide Molecules: Morphology Control. *J. Am. Chem. Soc.* **128,** 7390–7398 (2006).
40. Hollamby, M. J. *et al.* Tri-Chain Hydrocarbon Surfactants as Designed Micellar Modifiers for Supercritical CO_2. *Angew. Chem. Int. Ed.* **48,** 4993–4995 (2009).
41. Ryoo, W., Webber, S. E. & Johnston, K. P. Water-in-Carbon Dioxide Microemulsions with Methylated Branched Hydrocarbon Surfactants. *Ind. Eng. Chem. Res.* **42,** 6348–6358 (2003).
42. Nurmawati, M. H., Ajikumar, P. K., Renu, R., Sow, C. H. & Valiyaveettil, S. Amphiphilic Poly(p-phenylene)-Driven Multiscale Assembly of Fullerenes to Nanowhiskers. *ACS Nano* **2,** 1429–1436 (2008).
43. Kawauchi, T. *et al.* Encapsulation of Fullerenes in a Helical PMMA Cavity Leading to a Robust Processable Complex with a Macromolecular Helicity Memory. *Angew. Chem. Int. Ed.* **47,** 515–519 (2008).
44. Tashiro, K. & Aida, T. Metalloporphyrin hosts for supramolecular chemistry of fullerenes. *Chem. Soc. Rev.* **36,** 189–197 (2007).
45. Giacalone, F. & Martín, N. New Concepts and Applications in the Macromolecular Chemistry of Fullerenes. *Adv. Mater.* **22,** 4220–4248 (2010).
46. Patterson, A. L. The Scherrer Formula for X-Ray Particle Size Determination. *Phys. Rev.* **56,** 978 (1939).

47. Hirata, S. *et al.* Improvement of Electroluminescence Performance of Organic Light-Emitting Diodes with a Liquid-Emitting Layer by Introduction of Electrolyte and a Hole-Blocking Layer. *Adv. Mater.* **23,** 889–893 (2011).
48. Babu, S. S. *et al.* Nonvolatile liquid anthracenes for facile full-colour luminescence tuning at single blue-light excitation. *Nat. Commun.* **4,** 1969 (2013).
49. Burghardt, S., Hirsch, A., Schade, B., Ludwig, K. & Böttcher, C. Switchable Supramolecular Organization of Structurally Defined Micelles Based on an Amphiphilic Fullerene. *Angew. Chem. Int. Ed.* **44,** 2976–2979 (2005).
50. Nierengarten, J.-F. Chemical modification of C_{60} for materials science applications. *New J. Chem.* **28,** 1177–1191 (2004).

Figure Legends

Figure 1: Micelle formation. (**a**) Chemical structure of molecule **1** and photograph of a solution in *n*-hexane, alongside a schematic representation of the cluster structure. (**b**) Visible absorption spectra for **1** with *n*-hexane for concentrations of **1** as indicated. The inset shows magnified spectra indicating the shift in the position of the maxima centred around 703 nm with increased concentration. (**c**) Cryo-TEM image of micelles of **1** in *n*-decane. The full image is provided in Supplementary Figure S2, alongside an image for *n*-decane alone. (**d**) SAXS and SANS data for **1** with *n*-hexane and *n*-hexane-d_{14} respectively, taken at 25 °C and [**1**] = 22 wt%. (inset) Proposed aggregate structure, indicating the parts highlighted by SAXS (C_{60}-rich core) and SANS (alkyl-rich shell).

Figure 2: Gel formation. (**a**) Chemical structure of **2** and (**b**) photographs showing the gelled and isotropic states that arise on adding *n*-alkanes to **2**. (**c**) Fitted synchrotron SAXS data for **2** with *n*-hexane, **2** at 20 wt%, taken at 5 °C (gel state) and 55 °C (isotropic state) respectively. Red lines indicate fits to the data. For clarity SAXS data and fit for the isotropic state have been divided by a factor of 5. (Inset, **c**) Schematic depictions of the structures (micelles or gel fibres) present in the system in both states.

Figure 3: Structure and photoconductivity of the gel fibres. (**a**) XRD data for the gelled state of 28.7 wt% **2** with *n*-hexane, taken at 0 °C. The broad peak at higher angles represents the alkyl content of **2** and *n*-hexane, as indicated. (inset, **a**) Polarized optical microscopy (POM) images of the gelled state without (w/o) and with crossed (x-ed) polarizing filters, as indicated. The scale bar is the same for both halves of the image. (**b**) Solution-state FP-TRMC data for 42 wt% **2** with *n*-decane, taken at 23 °C (gelled state, 12 hours aging) and 48 °C (isotropic state), λ_{ex} = 355 nm.

Figure 4: Lamellar mesophase formation, structure and photoconductivity. (**a**, **b**) POM images of blends of C_{60} and **1** in molar ratios 1:2 and 1:10 at room temperature. (**c**, **d**) Rheology data showing the change in complex viscosity η^*, storage modulus G', and loss

modulus *G''* values with angular frequency *ω*. The tests were carried out at 0.1% strain amplitude in the linear-viscoelastic region at 25 °C. (**e**) XRD data for both ratios, highlighting the different positions of labelled peaks ***I-V*** for the two ratios. (**f**) FP-TRMC data for the two ratios and for pure **1** in the solvent-free condensed phase, λ_{ex} = 355 nm.

Figure 5. Lamellar mesophase microstructure. (**a**) TEM image of lamellar mesophase formed in the blend of C_{60} and **1** in the molar ratios 1:10 at room temperature. (**b**) Magnified area, showing the interdigitated C_{60} units. (**c**) Fast Fourier transform (FFT) of the image shown in panel (**a**). Spots corresponding to the lamellar spacing (001, 002 and 003), and to the C_{60}-C_{60} separation are indicated.

Figure 6. Conceptual figure. Schematic illustration of the directed assembly method described in this study, highlighting the structures formed.

Author Contributions

MJH and TN are joint principal investigators – they designed the work, carried out research, analyzed data and wrote the paper. MK helped to characterise the lamellar mesophases; PHHB and NAJMS performed the cryo-TEM experiments; AS and SS performed the TRMC studies; H. Minamikawa contributed to the temperature-dependent XRD studies; IG, PB and JE helped acquire the SANS data and advised on presentation and English; BRP helped acquire, reduce and analyse the SAXS data. H. Möhwald was involved in the work discussion. All authors discussed the results and commented on the manuscript.

Supplementary Information

This section, which includes the experimental details, model fitting details, fit parameters and supplementary figures, is available online

Acknowledgements

This work was partially supported by KAKENHI (23685033, 25620069) from the MEXT, Japan. Additionally, MH thanks both the Japan Society for the Promotion of Science (JSPS) and NIMS International Center for Young Scientists (ICYS) for funding. The SPring-8 synchrotron radiation experiment was performed on BL40B2 with the approval the Japan Synchrotron Radiation Research Institute (JASRI) (Proposal No. 2011B1548). We acknowledge the beamline contact, N. Ohta (SPring8), for his help with performing the SAXS measurements. We also acknowledge H. Li (MPI), H. Ozawa, Y. Akasaka, M. Matsuda, J. Aimi and M. Takeuchi (NIMS) for helpful discussions, M. Ohnuma and T. Taguchi (NIMS) for use of the for Rigaku SAXS equipment and rheometer respectively, the Soft Materials Line and the MANA TSS group at NIMS for use of spectroscopic facilities, and the STFC and Institut Laue Langevin for beam-time on D11.